Available online at www.sciencedirect.com
SCIENCE DIRECT®
Journal of Solid State Chemistry 177 (2004) 725–730
JOURNAL OF SOLID STATE CHEMISTRY
http://elsevier.com/locate/jssc

New one-dimensional uranyl and neptunyl iodates: crystal structures of $K_3[(UO_2)_2(IO_3)_6](IO_3)\cdot H_2O$ and $K[NpO_2(IO_3)_3]\cdot 1.5H_2O$

Richard E. Sykora,[a] Amanda C. Bean,[a,b] Brian L. Scott,[b] Wolfgang Runde,[b] and Thomas E. Albrecht-Schmitt[a,*]

[a] *Department of Chemistry and Leach Nuclear Science Center, Auburn University, Auburn, AL 36849, USA*
[b] *Chemistry Division, Los Alamos National Laboratory, Los Alamos, NM 87545, USA*

Received 3 July 2003; received in revised form 12 August 2003; accepted 20 August 2003

Abstract

The uranyl and neptunyl(VI) iodates, $K_3[(UO_2)_2(IO_3)_6](IO_3)\cdot H_2O$ (**1**) and $K[NpO_2(IO_3)_3]\cdot 1.5H_2O$ (**2**), have been prepared and crystallized under mild hydrothermal conditions. The structures of **1** and **2** both contain one-dimensional $^1_\infty[AnO_2(IO_3)_3]^{1-}$ (An = U, Np) ribbons that consist of approximately linear actinyl(VI) cations bound by iodate anions to yield AnO_7 pentagonal bipyramids. The AnO_7 units are linked by bridging iodate anions to yield chains that are in turn coupled by additional iodate anions to yield ribbons. The edges of the ribbons are terminated by monodentate iodate anions. For **1** and **2**, K^+ cations and water molecules separate the ribbons from one another. In addition, isolated iodate anions are also found between $^1_\infty[UO_2(IO_3)_3]^{1-}$ ribbons in **1**. In order to aid in the assignment of oxidation states in neptunyl containing compounds, a bond-valence sum parameter of 2.018 Å for Np(VI) bound exclusively to oxygen has been developed with $b=0.37$ Å. Crystallographic data (193 K, Mo$K\alpha$, $\lambda=0.71073$): **1**, triclinic, $P\bar{1}$, $a=7.0609(4)$ Å, $b=14.5686(8)$ Å, $c=14.7047(8)$ Å, $\alpha=119.547(1)°$, $\beta=95.256(1)°$, $\gamma=93.206(1)°$, $Z=2$, $R(F)=2.49\%$ for 353 parameters with 6414 reflections with $I>2\sigma(I)$; (203 K, Mo$K\alpha$, $\lambda=0.71073$): 2, monoclinic, $P2_1/c$, $a=7.796(4)$ Å, $b=7.151(3)$ Å, $c=21.79(1)$ Å, $\beta=97.399(7)°$, $Z=4$, $R(F)=6.33\%$ for 183 parameters with 2451 reflections with $I>2\sigma(I)$.

Keywords: Hydrothermal synthesis; Uranyl iodate; Neptamyl iodal Actinides

1. Introduction

The vast majority of U(VI) solids have been found to contain the approximately linear uranyl dioxo cation, UO_2^{2+} [1,2]. The terminal nature of the oxo atoms of the uranyl cations creates a predilection for uranyl-containing solids to adopt layered structures, and Burns et al.'s 1996 survey of U(VI) minerals and inorganic phases demonstrates that 59% of these compounds are in fact two-dimensional. The heavier actinides neptunium and plutonium are also expected to conform to this trend since they too form actinyl(V) and actinyl(VI) cations [2], albeit substantial bonding differences can also occur, especially in the case of NpO_2^+ [3]. One-dimensional uranyl topologies are much less frequently encountered, and at the time of the aforementioned review only 11% of U(VI) phases were found to be one-dimensional [1].

One of the common themes of one-dimensional U(VI) architectures is the presence of an oxoanion with a stereochemically active lone-pair of electrons. The nonbonding nature of these electrons pairs can cause the loss of a second dimension of connectivity, thereby leading to the excision of one-dimensional features from two-dimensional topologies [4,5]. The minerals moctezumite, $PbUO_2(TeO_3)_2$ [6], derriksite, $Cu_4[(UO_2)(SeO_3)_2](OH)_6$ [7], demesmaekerite, $Pb_2Cu_5[(UO_2)(SeO_3)_3]_2(OH)_6(H_2O)_2$ [8], and the synthetic phase $UO_2(HSeO_3)_2(H_2O)$ [9] all contain oxoanions with a lone-pair of electrons, and these compounds display distinct one-dimensional uranium oxide topologies. Over the past several years, we have capitalized on the structural effects of this family of oxoanions to produce a large number of new one-dimensional uranyl selenite, tellurite, and iodate topologies in $UO_2(IO_3)_2$ [10],

*Corresponding author. Department of Chemistry, 179 Chemistry Building, Auburn University, AL 36849, USA. Fax: +1-344-844-6959.
E-mail address: albreth@auburn.edu (T.E. Albrecht-Schmitt).

0022-4596/$ - see front matter © 2003 Elsevier Inc. All rights reserved.
doi:10.1016/j.jssc.2003.08.027

$A_2[(UO_2)_3(IO_3)_4O_2]$ (A = K, Rb, Tl) [4,5], $AE[(UO_2)_2(IO_3)_2O_2](H_2O)$ (AE = Sr, Ba, Pb) [4,5], $Ca[UO_2(SeO_3)_2]$ [11], $Sr[UO_2(SeO_3)_2]\cdot 2H_2O$ [11], β-$Tl_2[(UO_2)_2(TeO_3)_2]$ [12], $Sr_3[UO_2(TeO_3)_2](TeO_3)_2$ [12], $A_2[UO_2(CrO_4)(IO_3)_2]$ (A = K, Rb, Cs) [13,14], $Rb[UO_2(CrO_4)(IO_3)(H_2O)]$ [14], $K_2[UO_2(MoO_4)(IO_3)_2]$ [14], and $Cs_2[(UO_2)_3Cl_2(IO_3)(OH)O_2]\cdot 2H_2O$ [15]. However, it should be noted that the aforementioned C_{3v} anions are not essential in the formation of one-dimensional chains and ribbons, and several new one-dimensional topologies are recognized to occur in parsonsite, $Pb_2[UO_2(PO_4)_2]$ [16], $Li(H_2O)[(UO_2)_2(O)(Cl)_3(H_2O)]$ [14], $Li_2[UO_2(MoO_4)_2]$ [17], $[C_4H_{12}N_2][UO_2(H_2O)(SO_4)_2]$ [18], $[C_5H_{14}N_2][UO_2(H_2O)(SO_4)_2]$ [18], $A_6[(UO_2)_2O(MoO_4)_4]$ (A = Na, K) [19], and in $UO_2(H_2AsO_4)_2\cdot H_2O$ [20] where tetrahedral oxoanions are present in lieu of anions with a pyramidal structure.

The diversity of topologies observed in one-dimensional uranyl compounds can be ascribed to the ability of U(VI) to bind between four and six additional atoms perpendicular to the uranyl axis, thus forming tetragonal bipyramidal [UO_6], pentagonal bipyramidal [UO_7], and hexagonal bipyramidal [UO_8] units. These units can corner and/or edge-share to yield extended structures, and can also be joined solely by bridging anions. When this structural flexibility is combined with the wide variety of binding modes that the employed oxoanions can adopt, very large families of compositionally similar, yet structurally divergent compounds can be developed. One such advance is disclosed in the structures of $K_3[(UO_2)_2(IO_3)_6](IO_3)\cdot H_2O$ (**1**) and $K[NpO_2(IO_3)_3]\cdot 1.5H_2O$ (**2**), both of which contain one-dimensional ribbons of uranyl or neptunyl(VI) cations bridged by iodate anions. The key difference between these compounds and the previously reported alkali metal uranyl iodates, $A_2[(UO_2)_3(IO_3)_4O_2]$ (A = K, Rb, Tl) [4,5] is the absence of bridging oxo groups within the ribbons of **1** and **2**.

2. Experimental

2.1. Syntheses

UO_3 (99.8%, Alfa-Aesar), KIO_4 (99.9%, Fisher), KOH (85.8%, Fisher), and V_2O_5 (99.95%, Alfa-Aesar) were used as received. A $^{237}Np(V)$ stock solution (0.1 M) was prepared by dissolution of $^{237}NpO_2$ in 3 M HCl, followed by subsequent precipitation with 1 M NaOH and dissolution of the washed precipitate in 0.5 M HCl. Distilled and millipore filtered water with a resistance of 18.2 MΩ cm was used in all reactions. Reactions were run in Parr 4749 10-mL or 23-mL autoclaves with PTFE liners. SEM/EDX analyses were performed using a JEOL 840/Link Isis instrument. U and K percentages were calibrated against standards. Typical results are within 3.5% of ratios determined from single crystal X-ray diffraction. *Warning*: *While the UO_3 contains depleted U, standard precautions for handling radioactive materials should be followed. Old sources of depleted U should not be used, as the daughter elements of natural decay are highly radioactive and present serious health risks. ^{237}Np was utilized in accordance with established practices at Los Alamos National Laboratory*.

$K_3[(UO_2)_2(IO_3)_6](IO_3)\cdot H_2O$ (**1**). UO_3 (171 mg, 0.60 mmol), KIO_4 (275 mg, 1.20 mmol), and V_2O_5 (54 mg, 0.30 mmol) were loaded into an autoclave followed by the addition of 0.5 mL of a 1.7 M KOH solution. The autoclave was heated at 180°C for 72 h, and slow cooled at 9°C/h to 22°C. No liquid remained in the autoclave after the reaction was completed. Yellow needles of **1** were recovered in addition to orange acicular crystals of $K_2[(UO_2)_2(VO)_2(IO_6)_2O]\cdot H_2O$ [21]. Yield for **1**: 65 mg (20% based on I). EDX analysis provided a K:U:I ratio of 3:2:7.

$K[NpO_2(IO_3)_3]\cdot 1.5H_2O$ (**2**). KIO_4 (51.5 mg, 0.73 mmol), KCl (54.2 mg, 0.73 mmol), and 500 μL of water were loaded in a 10-mL PTFE-lined autoclave followed by the addition of 200 μL of a 0.1 M $^{237}Np(V)$ stock solution. The autoclave was sealed, doubly contained in two heat-sealed Teflon bags, and placed in a box furnace pre-heated to 180°C. After 24 h the furnace was cooled at 13°C/h to 25°C. The product consisted of a light green solution over light green rectangular plates of **2**. Percent yield could not be established for this reaction owing to hazards associated with weighing dry solids containing transuranium elements.

2.2. Crystallographic studies

A single crystal of $K_3[(UO_2)_2(IO_3)_6](IO_3)\cdot H_2O$ (**1**) with dimensions of $0.034\times 0.040\times 0.400$ mm was mounted on a thin glass fiber with epoxy, secured on a goniometer head, cooled to −80°C with an Oxford Cryostat, and optically aligned on a Bruker SMART APEX CCD X-ray diffractometer using a digital camera. Intensity measurements were performed using graphite monochromated Mo$K\alpha$ radiation from a sealed tube with a monocapillary collimator. SMART was used for preliminary determination of the cell parameters and data collection control. The intensities of reflections of a sphere were collected by a combination of three sets of exposures (frames). Each set had a different ϕ angle for the crystal and each exposure covered a range of 0.3° in ω. A total of 1800 frames were collected with an exposure time per frame of 30 s for compound **1**. No crystal decay was observed during the data collection.

For **1**, determination of integral intensities and global cell refinement were performed with the Bruker SAINT (v 6.02) software package using a narrow-frame

integration algorithm. An analytical absorption correction [22] was applied followed by a semi-empirical absorption correction using SADABS [23]. The program suite SHELXTL (v 5.1) was used for space group determination (XPREP), structure solution (XS), and refinement (XL) [22]. K(1) and K(2) sites in **1** were found to be half-occupied. The final refinement included anisotropic displacement parameters for all atoms and a secondary extinction parameter.

A green plate of $K[NpO_2(IO_3)_3]\cdot 1.5H_2O$ (**2**) with dimensions of $0.050\times 0.100\times 0.200$ mm was sealed in a capillary, and the capillary was subsequently coated with clear nail polish. The crystal was cooled to −70°C using a Bruker LT-2 low-temperature device, and intensity data was collected on a Bruker P4/CCD/PC X-ray diffractometer. A similar data collection routine to that used for **1** was also used for **2** except that the frame exposure time was shortened to 10 s. The data were corrected for absorption using SADABS [23] and the structure was solved using aforementioned methods [22]. The final refinement included anisotropic displacement parameters on all atoms. The I(3) position in **2** was found to be disordered over two sites with occupancy of 50% for each site. This disorder might be indicative of symmetry reduction to $P2_1$, for instance. However, attempts to solve the structure in this and other space groups failed. Additional crystallographic details for **1** and **2** are listed in Table 1. Additional details can be found in the Auxiliary material.

Table 1
Crystallographic data for $K_3[(UO_2)_2(IO_3)_6](IO_3)\cdot H_2O$ (**1**) and $K[NpO_2(IO_3)_3]\cdot 1.5H_2O$ (**2**)

	Compound	
	$K_3[(UO_2)_2(IO_3)_6](IO_3)\cdot H_2O$	$K[NpO_2(IO_3)_3]\cdot 1.5H_2O$
Formula mass (amu)	1629.65	856.80
Color and habit	Yellow needle	Green tablet
Crystal system	Triclinic	Monoclinic
Space group	$P\bar{1}$ (No. 2)	$P2_1/c$ (No. 14)
a (Å)	7.0609(4)	7.796(4)
b (Å)	14.5686(8)	7.151(3)
c (Å)	14.7047(8)	21.79(1)
α (°)	119.547(1)	90
β (°)	95.256(1)	97.399(7)
γ (°)	93.206(1)	90
V (Å^3)	1301.43(12)	1204.3(9)
Z	2	4
T (°C)	–80	–70
λ (Å)	0.71073	0.71073
$2\theta_{max}$	56.58	56.22
ρ_{calcd} (g cm^{-3})	4.848	4.726
μ(Mo$K\alpha$) (cm^{-1})	213.16	167.22
$R(F)$ for $F_o^2>2\sigma(F_o^2)$[a]	0.0249	0.0633
$R_w(F_o^2)$[b]	0.0599	0.1433

[a] $R(F)=\sum||F_o|-F_c||/\sum|F_o|$.
[b] $R_w(F_o^2)=\left[\sum[w(F_o^2-F_c^2)^2]/\sum wF_o^4\right]^{1/2}$.

2.3. Bond valence calculations

The following exponential was used to calculate the bond-valence parameter, R_{ij}, for Np(VI) and oxygen [24,25].

$$R_{ij}=b\ln\left[V_i/\sum_j \exp(-d_{ij}/b)\right].$$

The valence, V_i, was fixed at 6 and the sums of valence contributions from all ligands bonded to Np were conducted using calculated bond lengths, d_{ij}, and a b value of 0.37 Å. The bond-valence parameter was calculated for each Np(VI) site and the values were averaged to obtain a final mean R_{ij}.

Data used to calculate the bond-valence parameter for Np(VI) were obtained from comprehensive searches for crystal structure reports using the Cambridge Structural Database (CSD), the Inorganic Crystal Structure Database (ICSD), SciFinder Scholar, Science Citation Index, and manual searches. Constraints were not placed on the R factors of reported structures, which were generally quite good. Disordered and suspicious structures were excluded from the calculation. Only structures that contained Np(VI) sites bonded exclusively to oxygen atoms were used in our calculations. A total of 12 crystallographically independent Np sites from 11 different crystal structures were used to calculate the bond-valence parameter. This parameter will likely improve as more Np(VI) structures become available, but enough data points were available for a meaningful determination of the bond-valence parameter [26].

3. Results and discussion

3.1. Syntheses

The reaction of UO_3 with KIO_4 and V_2O_5 under basic hydrothermal conditions results in the formation of $K_2[(UO_2)_2(VO)_2(IO_6)_2O]\cdot H_2O$ as the major product [21]. However, in some reactions a small amount of the IO_4^- anion is reduced by water to IO_3^-, which then reacts with uranyl cations in the presence of K^+ cations to yield small quantities of $K_3[(UO_2)_2(IO_3)_6](IO_3)\cdot H_2O$ (**1**). Under similar conditions aqueous NpO_2^+ can be reacted with KIO_4 and KCl to produce $K[NpO_2(IO_3)_3]\cdot 1.5H_2O$ (**2**). The IO_4^- anion acts as the oxidant ($E^\circ=1.601$ V) in this reaction and converts Np(V) to Np(VI) ($E^\circ=1.24$ V) [27].

3.2. Bond-valence sums for Np(VI)

The $An=O$ ($An=U$, Np, Pu, Am) bond distance in actinyl complexes is often used as the primary parameter

for determining the actinide oxidation state. We have found this bond distance to be too highly dependent on ligand type and coordination environment to make such a determination in some cases [12]. Instead, it is better to look at the total contribution of all atoms binding the actinide for evaluating its oxidation state, i.e. the bond-valence sum [24,25]. In a previous report on the structural chemistry of neptunyl(V) iodates and selenites, we developed the bond-valence parameter for the Np(V)–O bond [3b]. The bond-valence parameter, R_{ij}, calculated for Np(V) with $b = 0.37$ Å was 2.036 Å. The bond-valence parameter, R_{ij}, calculated for Np(VI), independent of coordination environment, with $b = 0.37$ Å was determined in this present study to be 2.018 Å.

3.3. Structures

$K_3[(UO_2)_2(IO_3)_6](IO_3)\cdot H_2O$ (**1**). The structure of **1** contains one-dimensional $^1_\infty[UO_2(IO_3)_3]^{1-}$ ribbons that propagate along the *a*-axis as shown in Fig. 1. These anionic chains are constructed from $[UO_7]$ pentagonal bipyramids linked together through bridging iodate groups. Monodentate iodate anions terminate the edges of the chains in **1** as also observed in $A_2[(UO_2)_3(IO_3)_4O_2]$ (A = K, Rb, Tl) [4,5], $AE[(UO_2)_2(IO_3)_2O_2](H_2O)$ (AE = Sr, Ba, Pb) [4,5], $A_2[UO_2(CrO_4)(IO_3)_2]$ (A = K, Rb, Cs) [13,14], and $K_2[UO_2(MoO_4)(IO_3)_2]$ [14]. Dissecting the chains into simpler structural units leads to a more thorough understanding of the structural chemistry involved. First, each uranyl, UO_2^{2+}, moiety is bound by five iodate anions, four bridging and one terminal. Three uranyl units are connected by three bridging iodate anions to form 12-member rings. Each ring then connects with an additional ring through three bridging iodate groups. The seven-coordinate environment of each U(VI) atom is completed by the monodentate iodate that serves to terminate the edges of the ribbon. The anionic ribbons are separated by IO_3^- anions, K^+ cations, and water molecules. The packing diagram for **1** is shown in Fig. 2. Ionic $K^+\cdots O$ contacts, ranging from 2.600(5) to 3.387(5) Å, are formed with the water molecules and iodate anions. The occluded water molecule also forms hydrogen bonds with terminal oxo atoms from the iodate anions within the $^1_\infty[UO_2(IO_3)_3]^{1-}$ ribbons.

There are two crystallographically unique uranyl cations in **1** whose unremarkable U = O bond distances range from 1.778(4) to 1.796(4) Å. The U–O bond lengths within the equatorial planes of these $[UO_7]$ units vary from 2.282(4) to 2.397(3) Å. These distances have been used to calculate the bond-valence sum of the uranium centers in **1** with values of 6.09 and 6.04 being found for U(1) and U(2), respectively [1a]. There is no correlation between the U–O distance and the nature of the binding mode of the iodate anion, e.g. the monodentate iodate U–O distances are not notably longer or shorter than those to bridging iodate anions. In contrast the I–O bond distances do show systematic variations based on whether the oxo atoms are terminal or used to bind the uranyl moieties. There are seven crystallographically unique iodate anions, six of which are contained within the $^1_\infty[UO_2(IO_3)_3]^{1-}$ ribbons. The I–O bond distances vary from 1.765(4) to 1.849 (4) Å. However, these distances can be separated into groups of terminal and bridging distances. The terminal I–O bond distances then only vary from 1.765(4) to 1.797(4) Å, whereas the bridging distances occur from 1.816(4) to 1.849(4) Å. The isolated IO_3^- anion has close to uniform I–O bond distances ranging from 1.801(4) to 1.808(4) Å. A key feature of these anions is the possibility of the net alignment of the stereochemically active lone-pair of electrons along a single polar axis as occurs in $NpO_2(IO_3)$ [3b] and $PuO_2(IO_3)_2\cdot H_2O$ [28]. The centrosymmetric space group of **1** precludes overall

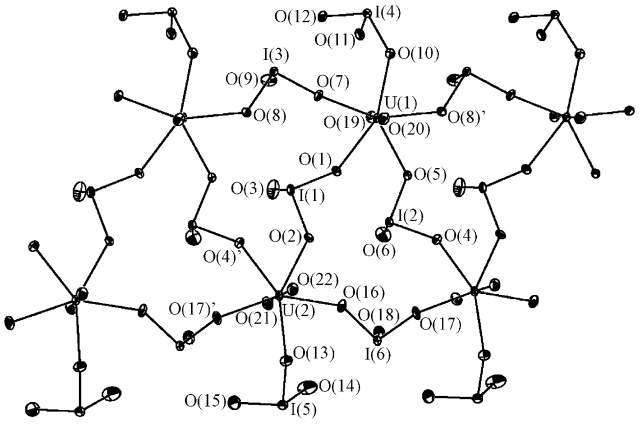

Fig. 1. A view of part of a one-dimensional, anionic $^1_\infty[UO_2(IO_3)_3]^{1-}$ ribbon in $K_3[(UO_2)_2(IO_3)_6](IO_3)\cdot H_2O$ (**1**). 50% probability ellipsoids are depicted.

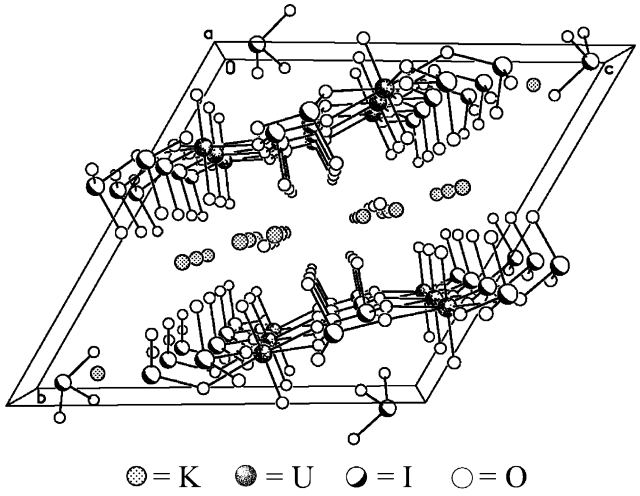

Fig. 2. An illustration of the unit cell and packing in $K_3[(UO_2)_2(IO_3)_6](IO_3)\cdot H_2O$ (**1**).

Table 2
Selected bond distances (Å) for $K_3[(UO_2)_2(IO_3)_6](IO_3)\cdot H_2O$ (**1**)

Bond lengths (Å)			
U(1)–O(1)	2.397(3)	U(2)–O(2)	2.381(4)
U(1)–O(5)	2.343(4)	U(2)–O(4)′	2.353(4)
U(1)–O(7)	2.282(4)	U(2)–O(13)	2.334(4)
U(1)–O(8)′	2.364(4)	U(2)–O(16)	2.331(4)
U(1)–O(10)	2.351(4)	U(2)–O(17)′	2.358(4)
U(1)═O(19)	1.778(4)	U(2)═O(21)	1.781(4)
U(1)═O(20)	1.796(4)	U(2)═O(22)	1.797(4)
I(1)–O(1)	1.824(3)	I(4)–O(12)	1.796(4)
I(1)–O(2)	1.822(4)	I(5)–O(13)	1.833(4)
I(1)–O(3)	1.770(4)	I(5)–O(14)	1.772(4)
I(2)–O(4)	1.838(4)	I(5)–O(15)	1.793(4)
I(2)–O(5)	1.820(4)	I(6)–O(16)	1.819(4)
I(2)–O(6)	1.765(4)	I(6)–O(17)	1.817(4)
I(3)–O(7)	1.816(4)	I(6)–O(18)	1.775(4)
I(3)–O(8)	1.833(3)	I(7)–O(23)	1.808(4)
I(3)–O(9)	1.792(4)	I(7)–O(24)	1.801(4)
I(4)–O(10)	1.849(4)	I(7)–O(25)	1.804(4)
I(4)–O(11)	1.797(4)		

polarity; however, the pyramidal iodate anions do show net alignment on one side of individual $^1_\infty[UO_2(IO_3)_3]^{1-}$ ribbons. Additional selected bond distances can be found in Table 2.

$K[NpO_2(IO_3)_3]\cdot 1.5H_2O$ (**2**). The structure of **2** contains ribbons similar to those found in **1**, and these can therefore be formulated as $^1_\infty[NpO_2(IO_3)_3]^{1-}$. The primary difference between **1** and **2** are the orientations of the iodate anions within the ribbons. As previously stated, each $^1_\infty[UO_2(IO_3)_3]^{1-}$ anionic ribbon is polar owing to the alignment of the stereochemically active lone-pair of electrons toward one side of the ribbon. However, in **2** we find that each ribbon is centrosymmetric with the iodate anions on one edge of the ribbon having the reverse polarity of those on the opposite edge. This unfortunately leads to the superposition of two orientations of the iodate anions that run down the center of the ribbons so that the I(3) position is disordered over two sites. This creates a number of deleterious effects in both the bond distances and angles about this particular anion, and we observe I–O bond distances varying from 1.808(15) to 1.97(2) Å, which are obviously not in reasonable agreement with what should be equivalent distances in **1**. A view of part of a disordered $^1_\infty[NpO_2(IO_3)_3]^{1-}$ ribbon, and a packing diagram for **2** are shown in Figs. 3 and 4, respectively. The two ordered IO_3^- anions fortunately show typical I–O bond distances that occur from 1.771(13) to 1.831(13) Å. These can be further subdivided as was done for **1** into terminal and bridging I–O distances to yield terminal distances from 1.771(13) to 1.789(13) Å and bridging distances from 1.802(17) to 1.831(13) Å. Given the lower resolution of **2** and the inherently larger errors, the statistical differences between these iodate distances becomes less significant. The K^+ cations form

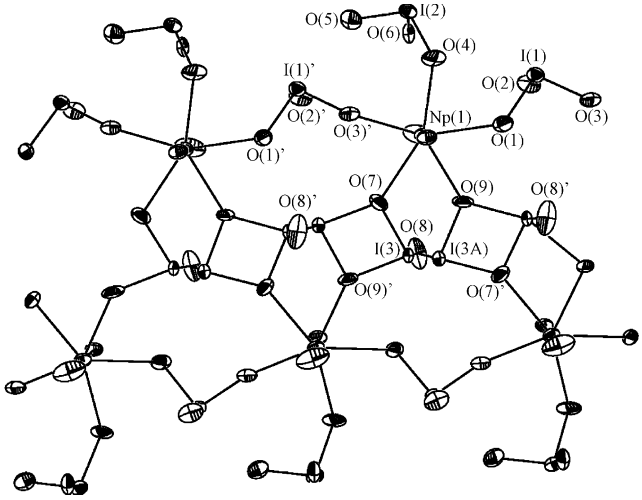

Fig. 3. A view of part of a disordered $^1_\infty[NpO_2(IO_3)_3]^{1-}$ ribbon in $K[NpO_2(IO_3)_3]\cdot 1.5H_2O$ (**2**). 50% probability ellipsoids are depicted.

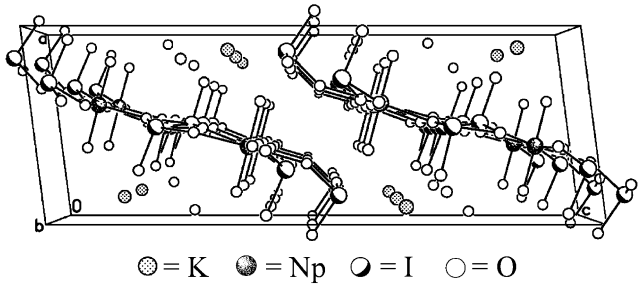

Fig. 4. An illustration of the packing of the K^+ cations, water molecules, and one-dimensional, anionic $^1_\infty[NpO_2(IO_3)_3]^{1-}$ ribbons in $K[NpO_2(IO_3)_3]\cdot 1.5H_2O$ (**2**).

Table 3
Selected bond distances (Å) for $K[NpO_2(IO_3)_3]\cdot 1.5H_2O$ (**2**)

Bond Lengths (Å)			
Np(1)–O(1)	2.394(17)	I(2)–O(4)	1.830(12)
Np(1)–O(3)	2.297(17)	I(2)–O(5)	1.788(16)
Np(1)–O(4)	2.311(13)	I(2)–O(6)	1.789(13)
Np(1)–O(7)	2.404(14)	I(3)–O(7)	1.919(16)
Np(1)–O(9)	2.324(15)	I(3)–O(8)	1.775(14)
Np(1)═O(10)	1.749(12)	I(3)–O(9)	1.968(19)
Np(1)═O(11)	1.762(15)	I(3A)–O(7)	1.926(16)
I(1)–O(1)	1.825(14)	I(3A)–O(8)	1.814(14)
I(1)–O(2)	1.772(13)	I(3A)–O(9)	1.893(16)
I(1)–O(3)	1.803(16)		

interactions with both terminal oxo atoms from the iodate anions and water molecules and also serve to separate the ribbons from one another. These $K^+\cdots O$ interactions range from 2.723(15) to 2.95(3) Å. Additional selected bond distances can be found in Table 3.

The central data points to be gleaned from the structure of **2** are the Np═O and Np–O bond distances within the $[NpO_7]$ pentagonal bipyramids. The Np═O bond distances within the NpO_2^{2+} unit are 1.749(12) and 1.761(15) Å, which are quite similar to the average

distance of 1.76(1) Å found in $NpO_2(IO_3)_2 \cdot H_2O$ and $NpO_2(IO_3)_2(H_2O)$ [29]. This correlation then leads to an oxidation state assignment of the neptunium in **2** as +6. The BVS for Np(1) can be calculated using aforementioned methods from the nepuntyl bond distances along with the Np–O bond distances, which range from 2.297(17) to 2.406(14) Å. These data provide a BVS of 6.14 for Np(1), which is consistent with Np(VI). In stark contrast to uranyl chemistry, the presence of a neptunyl unit often denotes an oxidation state other than VI. In fact, under typical oxidizing conditions found in groundwater, neptunium is more commonly found in the form of NpO_2^+, which contains Np(V) [30]. Therefore, the application of bond valence sum calculations to transuranium elements, especially neptunium and plutonium, is of substantial utility in many systems.

Auxiliary material

Further details of the crystal structure investigation may be obtained from the Fachinformationzentrum Karlsruhe, D-76344 Eggenstein-Leopoldshafen, Germany (Fax: (+49)7247-808-666; e-mail: crysdata@fiz-karlsruhe.de) on quoting depository numbers CSD 413239 and 413240.

Acknowledgments

This work was supported by the US Department of Energy, Office of Basic Energy Sciences, Heavy Elements Program (Grant DE-FG02-01ER15187). This research was also supported by the Environmental Management Science Program, Office of Science and Technology, US Department of Energy. Los Alamos National Laboratory is operated by the University of California for the US Department of Energy under Contract W-7405-ENG-36.

References

[1] (a) P.C. Burns, R.C. Ewing, F.C. Hawthorne, Can. Mineral. 35 (1997) 1551;
(b) P.C. Burns, in: P.C. Burns, R. Finch (Eds.), Uranium: Mineralogy, Geochemistry and the Environment, Mineralogical Society of America, Washington, DC, 1999 (Chapter 1);
(c) P.C. Burns, M.L. Miller, R.C. Ewing, Can. Mineral. 34 (1996) 845.
[2] F. Weigel, J.A. Fahey, J.J. Katz, G.T. Seaborg, in: J.J. Katz, G.T. Seaborg, J.R. Morss (Eds.), The Chemistry of the Actinide Elements, Chapman & Hall, London, 1986 (Chapter 5–7).
[3] (a) A. Cousson, S. Dabos, H. Abazli, F. Nectoux, M. Pagès, G. Choppin, J. Less-Common Metals 99 (1984) 233;
(b) T.E. Albrecht-Schmitt, P.M. Almond, R.E. Sykora, Inorg. Chem. 42 (2003) 3788;
(c) M.S. Grigor'ev, A.I. Yanovskii, Yu. T. Struchkov, A.A. Bessonov, T.V. Afonas'eva, N.N. Krot, Radiokhimiya 31 (1989) 37;
(d) N.N. Krot, D.N. Suglobov, Radiokhimiya 31 (1989) 1.
[4] A.C. Bean, T.E. Albrecht-Schmitt, J. Solid State Chem. 161 (2001) 416.
[5] A.C. Bean, M. Ruf, T.E. Albrecht-Schmitt, Inorg. Chem. 40 (2001) 3959.
[6] G.H. Swihart, P.K.S. Gupta, E.O. Schlemper, M.E. Back, R.V. Gaines, Am. Mineral. 78 (1993) 835.
[7] D. Ginderow, F. Cesbron, Acta Crystallogr. C 39 (1983) 1605.
[8] D. Ginderow, F. Cesbron, Acta Crystallogr. C 39 (1983) 824.
[9] V.E. Mistryukov, Y.N. Michailov, Koord. Khim. 9 (1983) 97.
[10] A.C. Bean, S.M. Peper, T.E. Albrecht-Schmitt, Chem. Mater. 13 (2001) 1266.
[11] P.M. Almond, S.M. Peper, E. Bakker, T.E. Albrecht-Schmitt, J. Solid State Chem. 168 (2002) 358.
[12] P.M. Almond, T.E. Albrecht-Schmitt, Inorg. Chem. 41 (2002) 5495.
[13] R.E. Sykora, S.M. McDaniel, D.M. Wells, T.E. Albrecht-Schmitt, Inorg. Chem. 41 (2002) 5126.
[14] R.E. Sykora, D.M. Wells, T.E. Albrecht-Schmitt, Inorg. Chem. 41 (2002) 2304.
[15] A.C. Bean, Y. Xu, J.A. Danis, T.E. Albrecht-Schmitt, W. Runde, Inorg. Chem. 41 (2002) 6775.
[16] P.C. Burns, Am. Mineral. 85 (2000) 801.
[17] S.V. Krivovichev, P.C. Burns, Solid State Sci. 5 (2003) 481.
[18] A.J. Norquist, P.M. Thomas, M.B. Doran, D. O'Hare, Chem. Mater. 14 (2002) 5179.
[19] S.V. Krivovichev, P.C. Burns, Can. Mineral. 39 (2001) 197.
[20] T.M. Gesing, C.H. Rüscher, Z. Anorg. Allg. Chem. 626 (2000) 1414.
[21] R.E. Sykora, T.E. Albrecht-Schmitt, Inorg. Chem. 42 (2003) 2179.
[22] G.M. Sheldrick, SHELXTL PC, Version 5.0, An Integrated System for Solving, Refining, and Displaying Crystal Structures from Diffraction Data, Siemens Analytical X-ray Instruments, Inc., Madison, WI, 1994.
[23] R.H. Blessing, SADABS. Program for absorption correction using SMART CCD based on the method of Blessing, Acta Crystallogr. A 51 (1995) 33.
[24] I.D. Brown, D. Altermatt, Acta Crystallogr. B 41 (1985) 244.
[25] N.E. Brese, M. O'Keeffe, Acta Crystallogr. B 47 (1991) 192.
[26] P.L. Roulhac, G.J. Palenik, Inorg. Chem. 42 (2003) 188.
[27] J.J. Katz, L.R. Morss, G.T. Seaborg, in: J.J. Katz, G.T. Seaborg, J.R. Morss (Eds.), The Chemistry of the Actinide Elements, Chapman & Hall, London, 1986 (Chapter 14).
[28] W. Runde, A.C. Bean, T.E. Albrecht-Schmitt, B.L. Scott, Chem. Commun. 4 (2003) 478.
[29] A.C. Bean, B.L. Scott, W. Runde, T.E. Albrecht-Schmitt, Inorg. Chem. 42 (2003) 5632.
[30] J.P. Kaszuba, W.H. Runde, Environ. Sci. Technol. 33 (1999) 4427.